J Appl Electrochem (2015) 45:577–583
DOI 10.1007/s10800-015-0812-5

RESEARCH ARTICLE

Fibroin nanofibrils as an electrode material for electrical double-layer biosupercapacitor applications

N. Sattarahmady[1,2] · R. Dehdari Vais[3] · H. Heli[3,4]

Received: 16 January 2015 / Accepted: 9 March 2015 / Published online: 17 March 2015

Abstract Fibroin nanofibrils were synthesized by a pH-controlled heat denaturation method. The nanofibrils were then applied to the surface of a carbon paste electrode to prepare a novel and biocompatible electrode for electrical double-layer supercapacitor applications. The capacity per surface area at a charge/discharge current of 1.0 A was obtained as 4.68 mF cm^{-2}. The electrode showed improved capability and charge/discharge behavior.

Keywords Electrical double-layer supercapacitor · Fibroin · Nanofibrils · Biosupercapacitor

1 Introduction

Supercapacitors are high performance electrochemical energy storage devices, which have received interest for different applications in electronic vehicles and circuits and backup power devices. Electrical double-layer supercapacitors (EDLSCs), as high performance electrochemical energy storage systems, store energy as an electric field in a dielectric medium to supply a high specific power with long cycling stability and high currents. EDLSCs store energy mainly in the electrical double layer which is formed at the electrode/electrolyte interface via reversible adsorption of ions at the electrode surface.

To fabricate EDLSCs electrodes, carbonaceous materials including graphite [1], carbon black [2], high porosity carbons [3], carbon fibers [4], carbon nanotubes [5], carbon aero-, xero-, and cryo-gels [6–8], fullerenes [9], and graphene [10] have been employed. On the other hand, by immobilization of a high density of charged species on the electrode surface, the charge and capacity can be increased.

Integrating biology with material researches causes employment of biomolecules in fabrication of new tools and devices. For this purpose, immobilization of biomacromolecules at the surface leads to interesting properties and applications in biosensors, bioelectronics, biomaterials, implants, tissue engineering, and energy-related devices [11–16]. In this regard, biomacromolecules of proteins [12], enzymes [17], and DNA [15] were immobilized on different surfaces. Most of these biodevices utilize external power sources or conventional energy storage [18, 19]. However, it is needed to develop energy storage devices that satisfy the biocompatibility, non-cytotoxicity, environmental friendly, and long-term functionality [16, 19]. The most well-known biocapacitor is the lipid bilayer membranes storing energy as an ionic charge separation across the insulating bilayer. Discharging of this membrane is employed for transduction of energy and signal processing. However, it is challenging to develop biocapacitors in vitro. On the other hand, supercapacitors that are fabricated by immobilizing nanosized biomaterials and employ aqueous electrolytes provide an enhanced surface charge in a biocompatible manner and have a high specific capacity, power density, rate capability, and safety [20, 21]. Along this line, DNA [22–25], c-type cytochrome electrically conductive microbial biofilm [25],

✉ H. Heli
hheli7@yahoo.com; heli@sums.ac.ir

1 School of Pharmacy, Pharmaceutical Science Research Center, Shiraz University of Medical Sciences, Shiraz, Iran

2 Department of Medical Physics, School of Medicine, Shiraz University of Medical Sciences, Shiraz, Iran

3 Nanomedicine and Nanobiology Research Center, Shiraz University of Medical Sciences, Shiraz, Iran

4 Department of Nanomedicine, School of Advanced Medical Sciences and Technologies, Shiraz University of Medical Sciences, Shiraz, Iran

albumin nanoparticles [16], and bioinspired peptide nanotubes [26] have been employed to fabricate EDLSC electrodes.

Silk fibroin has a variety of biomedical applications, including preparation of gels, sponges, and films [27], drug delivery [28], biosensors [29], bone formation [30], and regenerative medicine [31]. The amino acids' building blocks of fibroin are ionically charged and cause to formation of accumulated-charge surfaces, when it is immobilized. Immobilized fibroin can provide a high local charge density with a high ionic conductivity.

In the present work, a carbon paste electrode (CPE) was covered by nanofibrils of fibroin for EDLSC applications.

2 Materials and methods

2.1 Materials

All chemicals were of analytical grade form Merck and were used without further purification. Cocoons of Bombyx Mori were purchased from a local store. Graphite fine powder with an average size of <50 μm was received from Merck. All solutions were prepared with doubly distilled water.

2.2 Extraction of silk fibroin

Cocoons of Bombyx Mori were cut into small pieces and degummed twice by boiling, 20 min each, in an aqueous solution of 0.02 M Na_2CO_3 in order to remove glue-like silk sericin proteins and wax and then rinsed thoroughly with distilled water. Degummed silk was then thoroughly washed with distilled water and dried briefly at 37 °C. The extracted silk fibroin was then dissolved in a ternary system of a mixed solution of calcium chloride, ethanol, and water ($CaCl_2$:C_2H_5OH:H_2O of 1:2:8 mol ratio) at 90 °C for 6 h. After that the silk fibroin–salts solution was centrifuged at 8000 rpm for 10 min. The filtered solution was dialyzed continuously for 48 h against running pure water to remove $CaCl_2$, smaller molecules, and some impurities using a cellulose semi-permeable membrane. After dialysis, the protein solution was centrifuged at 6000 rpm for 5 min to remove impurities, precipitated matter, and the aggregates that occurred during dialysis.

2.3 Preparation of fibroin fibrils

5 mL of 0.35 % (w/v) fibroin solution was prepared by dilution of 5 % (w/v) fibroin stock solution with distilled water. Then, the pH of this solution was adjusted at 1.6 with addition of a diluted HCl solution. The resulting mixture was then incubated at 70 °C for 24 h in oil bath. After the incubation, the nanofibrillar protein sample was diluted two times with distilled water. The nanofibrils were washed with redistilled water and suspend in water. The final suspension had a concentration of ≈ 3.5 μg μL^{-1}.

2.4 Preparation of supercapacitor electrodes

CPE was prepared by hand-mixing of graphite fine powder and mineral oil with an 80/20 % (w/w) ratio. The paste was carefully mixed and homogenized in an agate mortar for 20 min. The resulting paste was kept at room temperature in a desiccator. The paste was firmly packed into a cavity (2.0 mm diameter and 0.5 mm depth) at the end of a Teflon tube. Electrical contact was established by a copper wire connected to the paste in the inner hole of the tube. The electrode surface was gently smoothed by rubbing on a piece of weighing paper just prior to use. The supercapacitor electrode (FF-CPE) was prepared by covering a CPE with different volumes of a fibroin nanofibrils suspension in water, and the electrode surface was dried under an IR lamp.

2.5 Apparatus

Electrochemical measurements were carried out in a conventional three-electrode cell containing 100 mM Na-phosphate buffer solution, pH 7.4 (PBS) powered by an μ-Autolab type III potentiostat/galvanostat (The Netherlands). An Ag/AgCl, 3 M KCl, a glassy carbon rod and CPE or FF-CPE were used as the reference, counter and working electrodes, respectively. The system ran on a PC through GPES and FRA 4.9 softwares. In order to obtain information about the morphology and size of the fibroin nanofibrils, scanning electron microscopy (SEM) and atomic force microscopy (AFM) were performed. SEM was performed by the instrument Sceron Technology, AIS-2100, Korea and AFM by a JPK Instruments AG-Nano-Wizard II in ambient conditions operating in the non-contact mode.

3 Results and discussion

Figure 1 shows SEM micrographs of fibroin fibrils with different magnifications. At low magnifications, SEM micrographs show long amorphous fibrous fibrils with an apparent width of about 10 μm and length of up to several hundred μm. These fibrils relatively squirm and in some parts have a wide width. Also, some fila, particles, and agglomerated structures with different shapes are observed in the images. Higher magnification images indicate that the fibers themselves comprise highly packed nanofibrils of long (higher than some micrometers) length with about

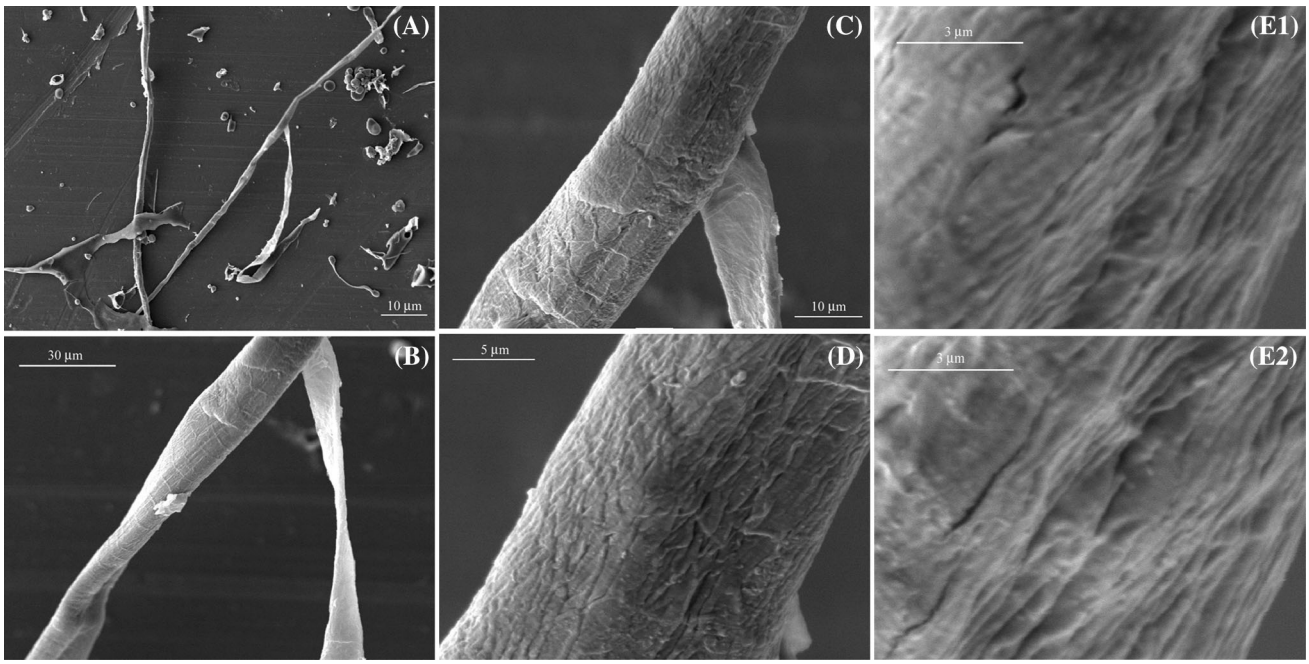

Fig. 1 SEM micrographs of fibroin fibrils with different magnifications

100 nm diameter, and a structure of "nanofibrils in fibrils" was formed through incubation of fibroin at low pH and high temperatures.

Figure 2 shows AFM images of fibroin fibrils with different magnifications. Patterns similar to those of SEM images appeared in AFM images. Fibroin fibrils with a substructure of nanofibrils are observed in the images.

In order to optimize the composition of FF-CPE, different CPEs covered with different volumes of the fibroin nanofibrils suspension were prepared. Figure 3 shows cyclic voltammograms of CPE and FF-CPEs prepared by covering 10, 20, 40, 50, 60, 70, and 80 µL of the nanofibrils suspension recorded in the range of 0–500 mV with a potential sweep rate of 50 mV s^{-1} in PBS. The voltammograms of all the electrodes are rectangular with a symmetric shape. In the swept range of potential, the fibroin components (amino acids) are not electroreactive, and only the charging currents are dominated indicating the characteristic of a capacitance in a combination with an Ohmic resistance [32]. In the voltammograms, the charging current for CPE is the lowest and that for FF-CPE with covering 60 µL of the fibroin nanofibrils suspension is the highest. Inset in Fig. 3 shows the dependency of the average capacitive current at 250 mV in the voltammograms on the volume of the fibroin nanofibrils suspension. Based on the data, the currents in the voltammograms increased up to 60 µL due to increment in the density of charged species on the surface and then decreased due to increment in the thickness of the fibroin layer (formation of a thick protein layer) and enhancement in the Ohmic drop [16]. Therefore, the volume of 60 µL of the fibroin nanofibrils suspension was selected to fabricate FF-CPE in further studies.

Figure 4a shows cyclic voltammograms of FF-CPE recorded at different potential sweep rates in PBS. Rectangular voltammograms are observed in all the potential sweep rates. Figure 4b shows the dependency of the anodic and cathodic currents sampled at the middle of the voltammogram as a function of the potential sweep rate. The linear dependency indicates that the currents are generated from the double-layer charging without contamination of any redox process. Figure 4c shows the variation of the total charge of the FF-CPE voltammograms as a function of the potential sweep rate. The variation in the electrode charge with the potential sweep rate is negligible. This indicates that the fibroin nanofibrils are adsorbed strongly and irreversibly on the CPE surface without significant desorption. On the other hand, the supercapacitive behavior of FF-CPE was attained at all the potential sweep rates.

According to the results, fibroin nanofibrils were adsorbed on the CPE surface and produced a fibroin nanofibrils-modified carbonaceous surface. Charge propagation through a thin film involves the dynamics of several processes that can overlap or influence themselves. In order to inspect the current pass through the protein-modified surface, two models of pinhole and membrane have been proposed [33, 34]. Based on the pinhole model, the adsorbed protein layer is impermeable, and ions and molecules can penetrate into the protein layer through some small pinholes.

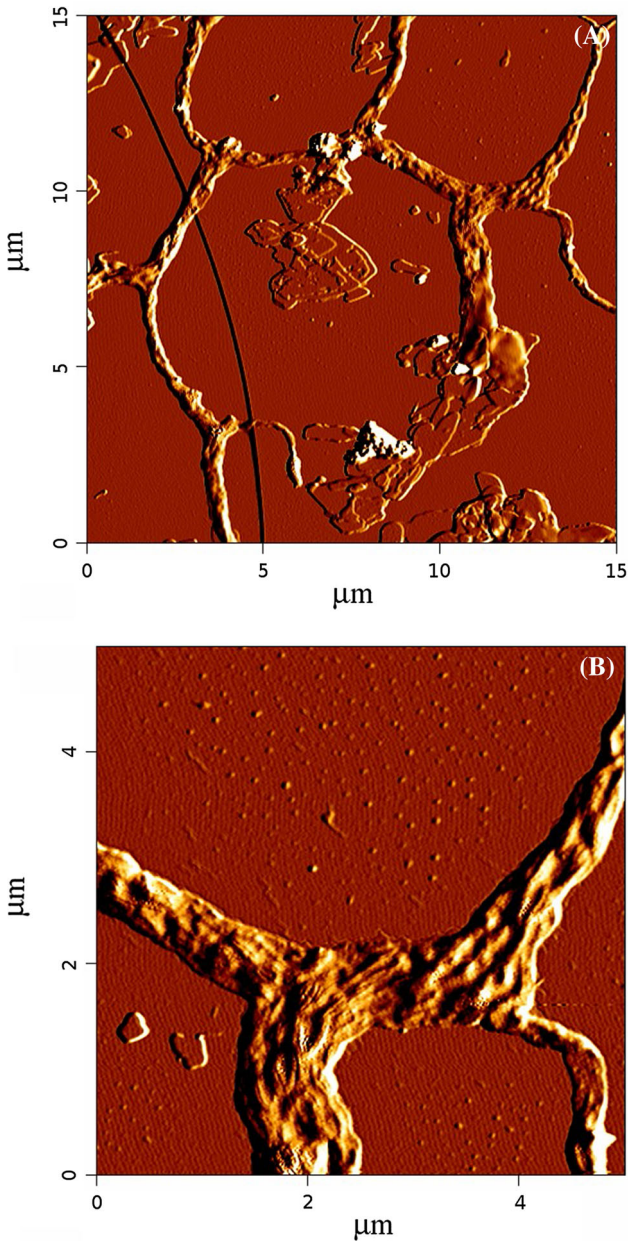

Fig. 2 AFM images of fibroin fibrils with different magnifications

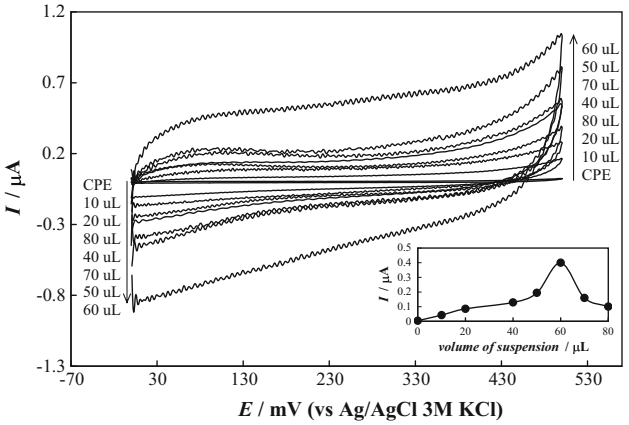

Fig. 3 Cyclic voltammograms of CPE and FF-CPEs prepared by covering 10, 20, 40, 50, 60, 70, and 80 µL of the nanofibrils suspension. The potential sweep rate was 50 mV s^{-1}. *Inset* The dependency of the average capacitive current of the voltammograms on the volume of the fibroin nanofibrils suspension

Alternatively, membrane model permits the protein layer to act as a uniform phase barrier with certain permeability. On the other hand, it has been reported that fibroin has a high affinity to be adsorbed on the carbonaceous surfaces, such as graphene and carbon nanotubes [35–37]. This attraction force is so outstanding and higher than the theoretical values expected [35]. The hydrogen bonding and polar–polar and hydrophobic–hydrophobic interactions have been reported to be the attraction forces between the silk fibroin (comprised polar random silk domains and the hydrophobic β-sheet nanocrystals) and the carbonaceous surfaces [35]. The affinity of the fibroin nanofibrils to the carbon surface is so high that even at electrostatic unfavorable conditions, the fibroin nanofibrils stay adsorbed on the surface. Fibroin, as a natural protein with the amino acids building blocks, provides an excellent medium with biocompatibility, thermal stability, and nontoxicity. The amino acids in the protein structure are charged and provide a high density of charged species immobilized on the surface. At the working pH, a net negative charge is assumed for the fibroin nanofibrils, due to the fibroin isoelectric point, pI = 3.6 [38] or pI = 1.4–2.8 [39]. The FF-CPE surface is covered by an ionic protein layer of negative charged which can provide a high-capacity double-layer capacitor.

Figure 5 shows Nyquist diagrams of CPE and FF-CPE recorded at the open circuit potential in PBS. Impedance curve for CPE contains a large arc followed by a line-like behavior at very low frequencies. This signature is a typical behavior of a blocking-type electrode/electrolyte interface toward the electron transfer process. The electrode does not represent redox reaction (appearance of a large arc), and a small-capacitance double-layer capacity is represented (the line at very low frequencies). On the other hand, the impedance curve for FF-CPE contains two linear parts. The high-frequency line has a slope of ≈2.3, and another near-vertical line appears at low frequencies. The signature of the impedance curve is characteristics of an anomalous diffusion [40], where the diffusing species is stopped for a period of time and the diffusion rate is slowed, followed by accumulation of ionic species in a thin layer (protein layer). The ionic charges are diffused inside the protein membrane and lead to provision of supercapacitive property.

Figure 6 represents typical galvanostatic charge/discharge plots for FF-CPE at different currents. A triangular feature is observed for all the plots including those recorded at high currents. This indicates that FF-CPE

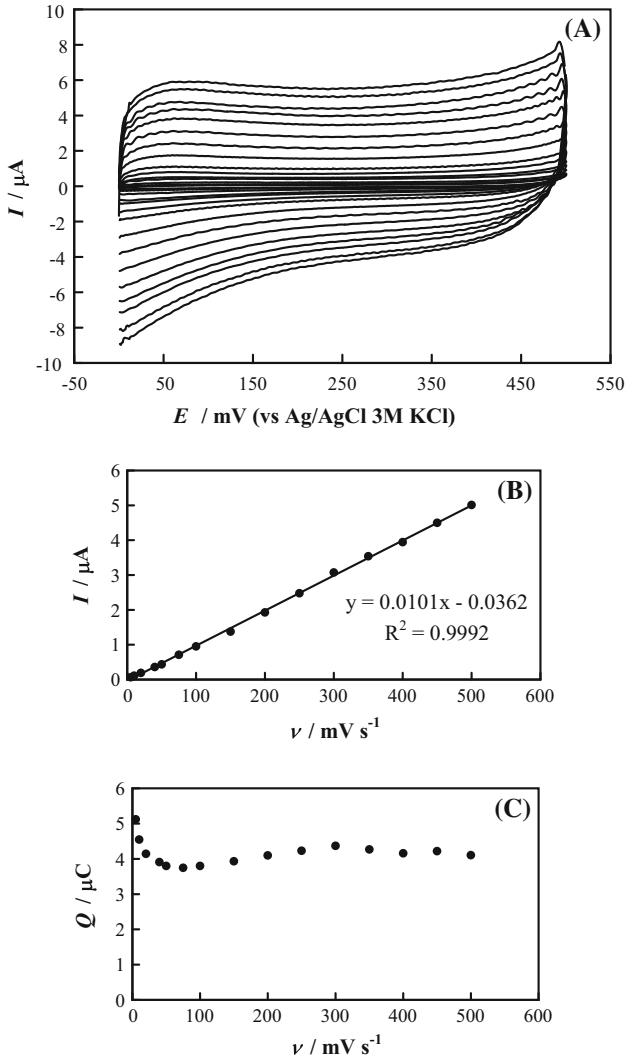

Fig. 4 **a** cyclic voltammograms of FF-CPE recorded at different potential sweep rates of 5, 10, 20, 40, 50, 75, 100, 150, 200, 250, 300, 350, 400, 450, and 500 mV s^{-1}. **b** Dependency of the anodic and cathodic currents sampled at the middle of the voltammograms as a function of the potential sweep rate. **c** Variation of the total charge of the FF-CPE voltammograms as a function of the potential sweep rate

represents an excellent electrochemical reversibility and charge/discharge behavior. From these galvanostatic charge/discharge plots, the FF-CPE capacitive behavior can be quantified. The specific capacitance is estimated as the capacity per weight (C_{sg}) and the capacity per surface area (C_{sa}), using the following equations:

$$C_{sg} = (I\Delta t)/(\Delta V m) \quad (1)$$

$$C_{sa} = (I\Delta t)/(\Delta V A), \quad (2)$$

where I, Δt, and ΔV are the charge/discharge current, the discharge time, and the potential change during the discharge process, respectively, and m and A are the mass and surface area of the active electrode material, respectively.

The values of the specific capacitance at different charge/discharge currents for FF-CPE are reported in Table 1. C_{sa} at a charge/discharge current of 1.0 μA was obtained as 4.68 mF cm^{-2} for FF-CPE, which is about 90 times higher than CPE. It has been reported that DNA can enhance two times the specific capacitance of pristine double-walled carbon nanotubes [23]. On the other hand, C_{sa} at a charge/discharge current of 1.0 μA for FF-CPE is about 6.8 times higher than G. sulfurreducens biofilm [25] and around 18 times higher than bioinspired peptide nanotubes [26]. Also, C_{sa} for FF-CPE is around six times higher than albumin nanoparticle-coated carbon electrode [16]. SEM and AFM results indicated that the fibrous fibrils had high surface area. These fibers contained much amino acid residues exposed upon fibril formation. Therefore, the fibers provide a high density of surface charge causing a high specific capacitance. It should be noted that the specific capacitance of FF-CPE is lower than the pseudocapacitors. In the pseudocapacitors, occurrence of redox reactions and employing the electrolyte solutions with higher ionic conductivities cause a highly specific capacitance. However, biocompatible supercapacitors should employ the electrolyte of physiologic pH (7.4). Therefore, the biosupercapacitors electrolyte will have limited ionic conductivity. Based on the data shown in Fig. 6, the values of *IR* drops in the charge/discharge plots at various currents are estimated, as shown in Fig. 6, inset. The linear dependency indicates that the *IR* drop in the electrode obeyed the Ohm's law. Therefore, the main resistance in FF-CPE is due to a constant resistive component inside the electrode materials.

The entity of the high capacity of FF-CPE can be related to two points. Fibroin nanofibrils provide a high ionic charge at the CPE surface; a high density of charged functional groups of amines and carboxylates is immobilized at the surface. On the other hand, fibroin nanofibrils provide a high real surface area on the CPE surface. These nanofibrils supply large pinholes and channels for the electrolyte ions to transport inside the electrode material.

Regarding the long-term stability of FF-CPE, 1000 consecutive charge/discharge curves were recorded. The results showed that the capacitance derived from charge/discharge curves changed <11 %. This indicates that FF-CPE had a good charge/discharge cycle stability.

4 Conclusion

We used a heat denaturation method at a low-pH solution to prepare fibroin nanofibrils. This method may be extendable to preparation of some other protein nanofibrils. Fibroin nanofibrils were immobilized at a surface and investigated with regard to supercapacitive properties.

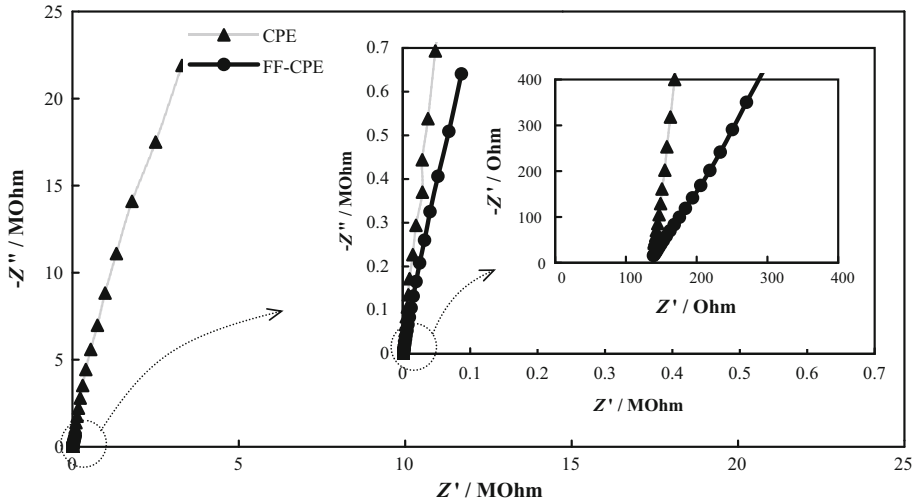

Fig. 5 Nyquist diagrams of CPE and FF-CPE recorded at open circuit potential in PBS

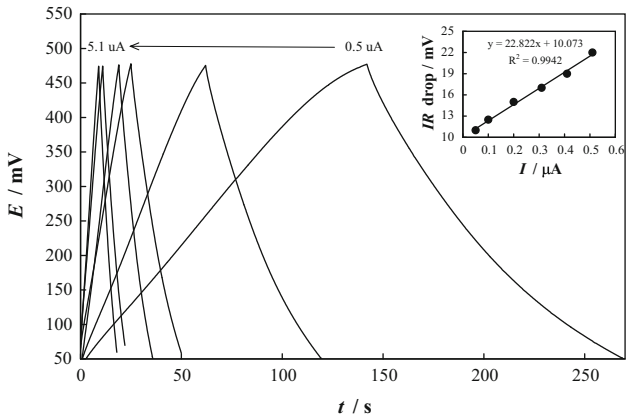

Fig. 6 Typical galvanostatic charge/discharge plots for FF-CPE at different currents of 0.5, 1.0, 2.0, 3.1, 4.1, and 5.1 μA. *Inset* Values of *IR* drops in the charge/discharge plots at various currents

Table 1 The values of specific capacitance for FF-CPE derived from the galvanostatic charge/discharge plots

I (μA)	Δt (s)	C_{sg} (F g^{-1})	C_{sa} (mF cm^{-2})
5.1	9	0.51	3.42
4.1	11	0.51	3.49
3.1	19	0.56	3.78
2.0	25	0.66	4.46
1.0	62	0.69	4.68
0.5	142	0.79	5.38

Immobilized fibroin nanofibrils at the surface, in one hand, provided immobilized charged sites, and on the other hand, provided pinholes and channels for water molecules and electrolyte ionic species to penetrate inside the protein layer on the electrode surface.

Acknowledgments We would like to thank the Research Council Shiraz University of Medical Sciences (5413) and the Iran National Science Foundation (INSF) for supporting this research.

References

1. Wang H, Yoshio M (2006) Graphite, a suitable positive electrode material for high-energy electrochemical capacitors. Electrochem Commun 8:1481–1486
2. Toupin M, Belanger D, Hill IR, Quinn D (2005) Performance of experimental carbon blacks in aqueous supercapacitors. J Power Sources 140:203–210
3. Weng CT, Teng H (2001) Characterization of high porosity carbon electrodes derived from mesophase pitch for electric double-layer capacitors. J Electrochem Soc 148:A368–A373
4. Yamazaki S, Takegawa A, Kaneko Y, Kadokawa J, Yamagata M, Ishikawa M (2009) An acidic cellulose-chitin hybrid gel as novel electrolyte for an electric double layer capacitor. Electrochem Commun 11:68–70
5. Kim YT, Mitani T (2006) Competitive effect of carbon nanotubes oxidation on aqueous EDLC performance: balancing hydrophilicity and conductivity. J Power Sources 158:1517–1522
6. Sepehri S, Garcia BB, Zhang Q, Cao G (2009) Enhanced electrochemical and structural properties of carbon cryogels by surface chemistry alteration with boron and nitrogen. Carbon 47:1436–1443
7. Skowronski JM, Osinska M (2012) Effect of nickel catalyst on physicochemical properties of carbon xerogels as electrode materials for supercapacitor. Curr Appl Phys 12:911–918
8. Halama A, Szubzda B, Pasciak G (2010) Carbon aerogels as electrode material for electrical double layer supercapacitors-Synthesis and properties. Electrochim Acta 55:7501–7505
9. Okajima K, Ikeda A, Kamoshita K, Sudoh M (2005) High rate performance of highly dispersed C_{60} on activated carbon capacitor. Electrochim Acta 51:972–977
10. Chen Y, Zhang X, Zhang D, Yu P, Ma Y (2011) High performance supercapacitors based on reduced graphene oxide in aqueous and ionic liquid electrolytes. Carbon 49:573–580
11. Ma PX (2008) Biomimetic materials for tissue engineering. Adv Drug Deliv Rev 60:184–198
12. Heli H, Sattarahmady N, Jabbari A, Moosavi-Movahedi AA, Hakimelahi GH, Tsai FY (2007) Adsorption of human serum albumin onto glassy carbon surface—applied to albumin-

modified electrode: mode of protein-ligand interactions. J Electroanal Chem 610:67–74
13. Kurella A, Dahotre NB (2005) Review paper: surface modification for bioimplants: the role of laser surface engineering. J Biomater Appl 20:5–50
14. Schelfer F, Schubert F (1992) Biosensors. Elsevier, Amsterdam
15. Heli H, Moosavi-Movahedi AA, Jabbari A, Ahmad F (2007) An electrochemical study of safranin O binding to DNA at the surface. J Solid State Electrochem 11:593–599
16. Sattarahmady N, Parsa A, Heli H (2013) Albumin nanoparticle-coated carbon composite electrode for electrical double-layer biosupercapacitor applications. J Mater Sci 48:2346–2351
17. Sassolas A, Blum LJ, Leca-Bouvier BD (2012) Immobilization strategies to develop enzymatic biosensors. Biotechnol Adv 30:489–511
18. Bettinger CJ, Bao Z (2010) Organic thin-film transistors fabricated on resorbable biomaterial substrates. Adv Mater 22:651–655
19. Onuki Y, Bhardwaj U, Papadimitrakopoulos F, Burgess DJ (2008) A review of the biocompatibility of implantable devices: current challenges to overcome foreign body response. J Diabetes Sci Technol 2:1003–1015
20. Nam KT, Kim DW, Yoo PJ, Chiang CY, Meethong N, Hammond PT, Chiang YM, Belcher AM (2006) Virus-enabled synthesis and assembly of nanowires for lithium ion battery electrodes. Science 312:885–888
21. Lee YJ, Yi H, Kim WJ, Kang K, Yun DS, Strano MS, Ceder G, Belcher AM (2009) Fabricating genetically engineered high-power lithium-ion batteries using multiple virus genes. Science 324:1051–1055
22. Shin SR, Lee CK, So I, Jeon JH, Kang TM, Kee C, Kim SI, Spinks GM, Wallace GG, Kim SJ (2008) DNA-wrapped single-walled carbon nanotubes hybrid fibers for supercapacitors and artificial muscles. Adv Mater 20:466–470
23. Cooper L, Amano H, Hiraide M, Houkyou S, Jang IY, Kim YJ, Muramatsu H, Kim JH, Hayashi T, Kim YA, Endo M, Dresselhaus MS (2009) Freestanding, bendable, thin film for supercapacitors using DNA-dispersed double walled carbon nanotubes. Appl Phys Lett 95:Article Number 233104
24. Yamazaki S, Obata K, Okuhama Y, Matsuda Y, Yamagata M, Ishikawa M (2010) Application of activated carbon/DNA composite electrodes to aqueous electric double layer capacitors. J Power Sour 195:1753–1756
25. Malvankar NS, Mester T, Tuominen MT, Lovley DR (2012) Supercapacitors based on c-type cytochromes using conductive nanostructured networks of living bacteria. ChemPhysChem 13:463–468
26. Beker P, Koren I, Amdursky N, Gazit E, Rosenman G (2010) Bioinspired peptide nanotubes as supercapacitor electrodes. J Mater Sci 45:6374–6378
27. Tsukada M, Freddi G, Minoura N, Allara G (1994) Preparation and application of porous silk fibroin materials. J Appl Polym Sci 54:507–514
28. Wenk E, Wandrey AJ, Merkle HP, Meinel L (2008) Silk fibroin spheres as a platform for controlled drug delivery. J Control Release 132:26–34
29. Qian J, Liu Y, Liu H, Yu T, Deng J (1996) Characteristics of regenerated silk fibroin membrane in its application to the immobilization of glucose oxidase and preparation of a p-benzoquinone mediating sensor for glucose. Fresenius J Anal Chem 354:173–178
30. Sofia S, McCarthy MB, Gronowicz G, Kaplan DL (2001) Functionalized silk-based biomaterials for bone formation. J Biomed Mater Res 54:139–148
31. Ubaldo A, Ilaria DP, Anna C, Giuliano F (2011) Will silk fibroin nanofiber scaffolds ever hold a useful place in translational regenerative medicine? Int J Burn Trauma 1:27–33
32. Conway BE (1999) Electrochemical supercapacitors: scientific fundamentals and technological applications. Kluwer/Plenum, New York
33. Andrieux CP, Saveant JM (1992) In: Murray A (ed) Molecular design of electrode surfaces, techniques of chemistry. Wiley, New York
34. Bard AJ (1994) Integrated chemical systems: a chemical approach to nanotechnology. Wiley, New York
35. Hu K, Gupta MK, Kulkarni DD, Tsukruk VV (2013) Ultra-robust graphene oxide-silk fibroin nanocomposite membranes. Adv Mater 25:2301–2307
36. Pan H, Zhang Y, Hang Y, Shao H, Hu X, Xu Y, Feng C (2012) Significantly reinforced composite fibers electrospun from silk fibroin/carbon nanotube aqueous solutions. Biomacromolecules 13:2859–2867
37. Piri N, Mottaghitalab V, Arbab S (2013) Conductive regenerated silk fibroin composite fiber containing MWNTs. e-Polymers 13:67–81
38. Sookne AM, Harris M (1939) Electrophoretic studies of silk. J Res Natl Bur Stand 23:299–308
39. Hawley TG, Johnson TB (1930) The isoelectric point of silk fibroin. Ind Eng Chem 22:297–299
40. Bisquert J, Compte A (2001) Theory of the electrochemical impedance of anomalous diffusion. J Electroanal Chem 499(2001): 112–120